Environ Chem Lett (2011) 9:251–257
DOI 10.1007/s10311-010-0274-2

ORIGINAL PAPER

Photocatalytic degradation of phenol with mesoporous $TiO_{2-x}B_x$

Leyan Xiong · Longzhen Zheng · Jingpeng Xu · Dan Zheng · Junhua Li · Xinjia Li · Juan Sun · Qiang Liu · Liling Niu · Shaoming Yang · Jian Xia

Received: 21 May 2009 / Accepted: 4 January 2010 / Published online: 14 January 2010

Abstract We report a facile approach for preparing mesoporous boron-doped TiO_2 materials by combining the sol–gel process with the dehydration of glucose. Specifically a high surface carbon material was formed by dehydration of glucose, then used as template. This material and the TiO_2 dry gel were calcinated to produce porous TiO_2. The as-synthesized boron-doped TiO_2 was in pure anatase crystallite phase with high surface area. X-ray photoelectron spectroscopy (XPS) results showed that boron was incorporated into the anatase TiO_2 lattice to form $TiO_{2-x}B_x$. The absorption spectra of $TiO_{2-x}B_x$ extended into the visible region to 460 nm. The $TiO_{2-x}B_x$ exhibited much higher photocatalytic activity on phenol degradation than pure TiO_2. It showed that the phenol degradation by-products of $TiO_{2-x}B_x$ were different from that of pure TiO_2. Mechanism of the photocatalytic degradation of phenol at $TiO_{2-x}B_x$ was also proposed.

Keywords Mesoporous materials · Boron-doped TiO_2 · High surface area · Photocatalytic activity · Phenol degradation

L. Xiong · L. Zheng (✉) · D. Zheng · J. Li · X. Li · J. Sun · Q. Liu · L. Niu · S. Yang · J. Xia
Department of Chemistry and Chemical Engineering, East China Jiao Tong University, 330013 Nanchang, Jiangxi, People's Republic of China
e-mail: zlz@ecjtu.jx.cn

J. Xu
Jiangxi Institute of Analysis and Testing, 330029 Nanchang, Jiangxi, People's Republic of China

Introduction

The growing demand from society for disinfection and detoxification of polluted waters from different sources has lead in the last few decades to the development of new and more effective water purification technologies. TiO_2 is the most widely used material in the pollution control because of its efficiency, easily availability, non-toxicity, low cost, and chemical stability (Chen et al. 2005; Chenthamarakshan and Rajeshwar 2000; Hoffmann et al. 1995; Bavykin et al. 2006; Carp et al. 2004). However, this material is only active upon UV excitation because of its large energy band gap of 3.2 eV (Wold 1993), which limits its photoactivity to ultraviolet light. To utilize a wider range of the solar spectrum, the band gap needs to be narrowed. Doping TiO_2 with non-metal atoms is a promising strategy and has received much attention. Asahi et al. (2001) reported that doping TiO_2 with nitrogen can lower its band gap and shift its optical response to the visible region. Recent experimental and theoretical studies showed that the localized 2p states in N above the valence band lead to the absorption of visible light (Livraghi et al. 2006; Batzill et al. 2006; Di Valentin et al. 2007). Besides nitrogen, there are some other non-metal dopants such as C (Khan et al. 2002; Nakano et al. 2005; Xu and Khan 2007; Wang and Lewis 2005), S (Yu et al. 2005; Liu and Chen 2008; Nishijima et al. 2008; Chen and Burda 2008), F (Zhou et al. 2008; Xu et al. 2008; Wu et al. 2008; Ho et al. 2006) and P (Zheng et al. 2008; Lin et al. 2005) to extend the photocatalytic activity into the visible light region. More recently, B-doped TiO_2 has received growing attention because of its promotional effects in photocatalytic activity (Zhao et al. 2004; In et al. 2007; Zaleska et al. 2008; Yang et al. 2007; Lu et al. 2007).

Mesoporous materials with 2D and 3D structures are one of the most exciting new developments in material

science and technology. Due to their large surface area and 2–50 nm size scale, these materials have attracted great attention for nanotechnological applications, such as catalysts, supports, adsorbents, matrices for photochemical species, sensing devices, and so on (Soler-illia et al. 2002; Boettcher et al. 2007). Generally, mesoporous structures enhance diffusion of the reactants throughout the channels, offering more active sites for adsorption, and consequently increasing the reaction speed. However, there are a few reports on mesoporous TiO_2 doped with non-metals have been presented to date (Bettinelli et al. 2007; Huang et al. 2008; Soni et al. 2008). Doping with non-metals is generally performed at high temperature, while high-temperature treatment frequently results in partial collapse of the porous structure, which decreases the specific surface area of catalysts. Therefore, it is still a challenge to prepare TiO_2 visible light photocatalysts with high specific surface areas and simultaneously realize doping with non-metals, crystallization and formation of porous structures.

In this paper, porous carbon with high surface area, which was formed by the dehydration of glucose by concentrated sulfuric acid, was used as hard template. The photocatalytic activity of TiO_2 mesoporous materials doped with different ratio of boron was investigated. Different structural and chemical characterizations of the boron-doped TiO_2 materials were conducted to explore the relationship between the enhanced photocatalytic activity and the incorporation of boron. The mechanisms of photocatalytic degradation of phenol at TiO_2 and boron-doped TiO_2 were also proposed.

Experimental section

Materials

Tetrabutyl titanate, boron hydroxide, phenol, glucose, sulfuric acid, and other reagents were all analytical purity purchased from Shanghai Chemical Reagent Factory. Doubly distilled water was used throughout this study.

Preparation of mesoporous TiO_2 photocatalysts doped with different ratio of boron

$Ti(OC_4H_9)_4$ was used as the precursor for the preparation of mesoporous TiO_2. In a typical synthesis, 3.4 g $Ti(OC_4H_9)_4$ is dissolved in 20 ml ethanol solution. Under vigorous stirring, 40 ml 1 M H_2SO_4 and 30 g glucose were added to the solution and hydrolyzed for 12 h to form transparent TiO_2 sol–gel solution. Then 0, 0.007, 0.014, 0.021, 0.035, 0.049, 0.070, and 0.105 g boron hydroxide were added to the TiO_2 sol–gel solution, respectively, and aged for another 12 h. The wet gels were dried at 100°C for 24 h and formed black dry gels. In order to remove the carbon support and maintain the mesoporous structure, the black dry gels were calcined in a multisegment programmable furnace at a heating rate of 1°C min^{-1} up to 450°C, followed by maintaining 450°C for 4 h and then at a cooling rate of 1°C min^{-1} down to room temperature. After cooled down, the TiO_2 mesoporous materials doped with different ratio of boron were obtained. Energy-dispersive X-ray (EDX) analysis results showed that the boron doping levels of the samples were consistent with their initial concentrations in solutions.

Apparatus

X-ray diffraction (XRD) was carried out on a Japan Rigaku D/max-RA X-ray diffractometer using graphite monochromatized high-intensity Cu Kα radiation ($\lambda = 1.5418$ Å).

To measure the surface area of the samples, a Micromeritics TriStar 3000 was used to collect a partial adsorption isotherm at 77 K, with nitrogen as the adsorption gas over the pressure range (P/P_0) of 0.05–0.3. Prior to measurements, the samples were degassed under vacuum at room temperature for 48 h. The specific surface area was determined according to the Brunauer–Emmett–Teller (BET) method in the relative pressure (P/P_0) range of 0.08–0.18.

The morphology, size, and the composition of the samples were studied by transmission electron microscopy (TEM) using a JEOL microscope (1200 EX II) with energy-dispersive X-ray (EDX) analysis.

The X-ray photoelectron spectrum (XPS) was recorded on a VG ESCALAB MKII X-ray photoelectron spectrometer (VG Scientific, UK), using a monochromatic Mg Kα X-ray radiation (h$\nu = 1253.6$ eV) as the excitation source. Peak position was internally referenced to the C 1s peak at 285.0 eV.

The UV–vis absorption spectrum was recorded on a Lambda 35 UV/VIS Spectrometer (PerkinElmer Precisely., USA).

The photocatalytic reactions were performed using a closed system with an inner irradiation-type quartz reactor. A high-pressure mercury lamp (110 W, Shanghai Yamin) was the light source. The lamp was plunged in a quartz immersion well with cooling water. The temperature of the reaction cell was controlled in the temperature range of 30–50°C by cooling water.

Photocatalytic experiments

A total of 50 ml 1×10^{-3} M phenol solution and 0.3 g TiO_2 photocatalyst were charged to the reactor, and the content was continuously stirred. After 30 min of dark run, the high-pressure mercury lamp was turned on to initiate

the photocatalytic reaction. The dark run was carried out to ensure that the adsorption equilibrium was reached. When the lamp was turned on, the counting of reaction time started after 10 min. In this respect, it was assumed that the lamp already reached its maximum intensity. As all experimental runs were carried out in the same manner, the results were comparable. Furthermore, errors due to maximum light intensity were ignorable as the first sample was only collected at 10 min after the lamp was turned on. The sampling of the solution was carried out using a 1-ml pipet at a 20-min interval for 2 h. These samples were centrifugalized to separated solid photocatalyst and solution. Then, the centrifugal solution was immediately analyzed by UV–vis spectroscopy to determine the concentrations of remaining phenol and intermediate products.

Results and discussion

Characterizaion of the boron-doped TiO_2 mesoporous material

Figure 1a showed the TEM image of the boron-doped TiO_2 mesoporous material prepared by the porous carbon hard template method. The average size of the particles is about 10 nm. It can also be seen that there were a large number of non-ordered wormhole-like pores among the nanoparticles with pore size of about 10 nm. The surface area of the boron-doped TiO_2 mesoporous material was measured to be 146 m^2/g. For comparison, the TEM image of boron-doped TiO_2 prepared without using porous carbon hard template was shown in Fig. 1b. The particles were about 30–40 nm large with some aggregation in them. The surface area was measured to be 34 m^2/g. The results indicated that the porous carbon hard template acted an important role in forming TiO_2 mesoporous structures with high surface area.

The crystal structure of the boron-doped TiO_2 mesoporous material was investigated by X-ray diffraction (XRD). Figure 2 showed the XRD pattern recorded for the boron-doped TiO_2 mesoporous material, and all the diffraction peaks could be readily indexed to the anatase TiO_2, which were well fitted to the reported data (JCPDS 21-1272). The peaks appeared at $2\theta = 25.28$, 37.80, 48.05, 53.89, 55.06, and 62.69°, which correspond to the anatase (101), (004), (200), (105), (211), and (204) crystalline planes. Furthermore, the sizes of the boron-doped TiO_2 mesoporous material were evaluated from the full width at half-maximum (FWHM) of the major diffraction peaks (101) observed in Fig. 1 by Scherrer's formula. The mean crystallite size was ca. 10 nm, which was in accordance with the TEM results.

The boron-doped TiO_2 was further characterized by XPS analysis. Wide scan and narrow scans of Ti 2p and B 1s of the samples are shown in Fig. 3. The XPS signal of Ti $2p^{3/2}$ can be fitted as one peak at 458.1 eV. Compared to the binding energy of Ti^{4+} in pure anatase TiO_2

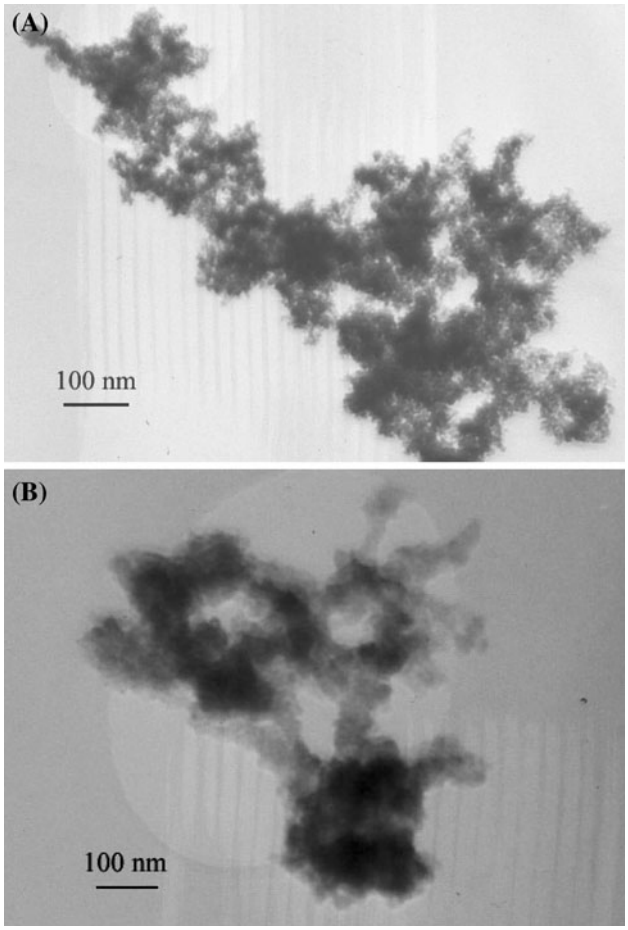

Fig. 1 TEM images of the prepared $TiO_{2-x}B_x$ using porous carbon hard template (**a**) and without using porous carbon hard template (**b**)

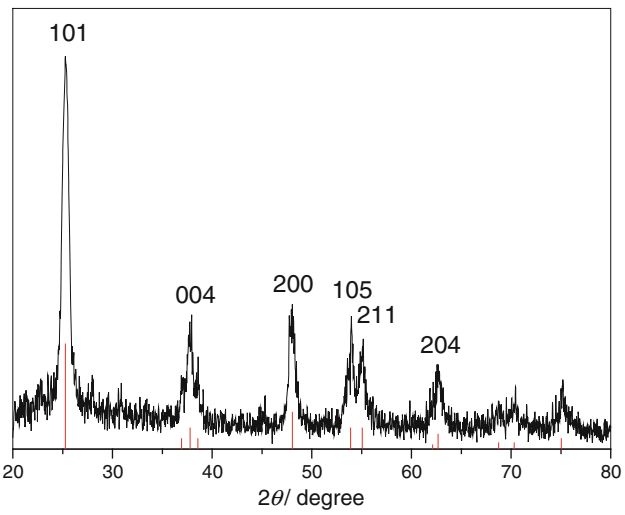

Fig. 2 XRD pattern of $TiO_{2-x}B_x$ mesoporous material

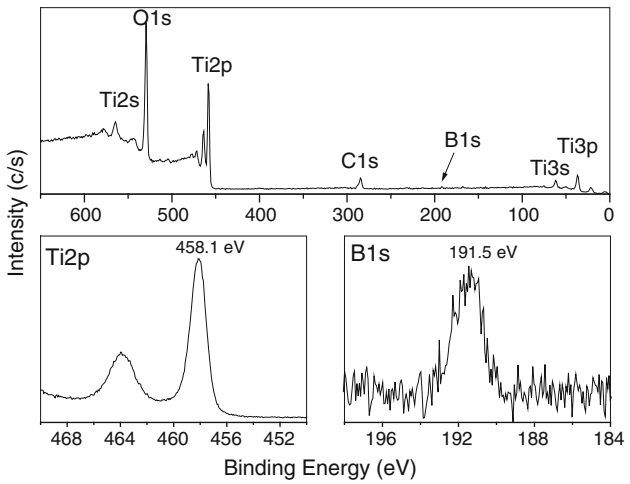

Fig. 3 XPS spectra of $TiO_{2-x}B_x$ mesoporous material

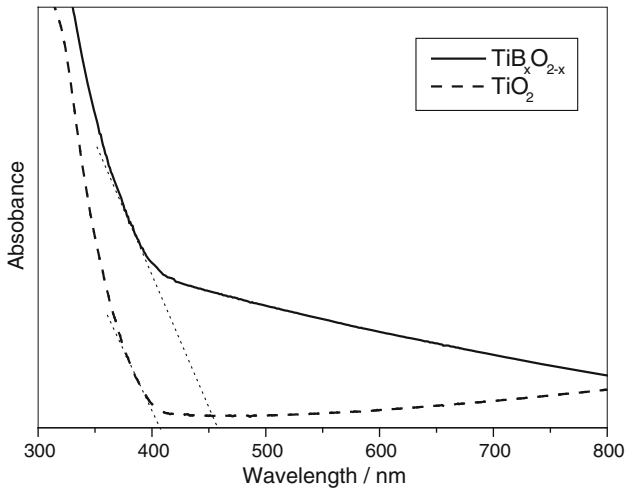

Fig. 4 UV–visible diffuse reflectance spectra of TiO_2 and $TiO_{2-x}B_x$

(458.6 eV), there was a red-shift of 0.5 eV for the boron-doped TiO_2, which suggested that Ti^{3+} species was formed in the boron-doped TiO_2 (Li et al. 2005). The binding energy for B 1s was shown as one peak at 191.5 eV, which is quite different from the binding energy of B_2O_3 (194.1 eV) and TiB_2 (188.2 eV) (Zhao et al. 2004). The XPS results indicated that the boron atom was incorporated into TiO_2 forming $TiO_{2-x}B_x$, rather than existing in a separate phase of B_2O_3 or forming intermetallic compound TiB_2.

Figure 4 showed the UV–vis diffuse reflectance absorption spectra of TiO_2 and $TiO_{2-x}B_x$ sample. Compared to TiO_2, the absorption of $TiO_{2-x}B_x$ sample extended significantly into the visible region from 410 to 460 nm. It was demonstrated clearly that the incorporation of boron into the anatase TiO_2 lattices resulted in a substantial red-shift of the absorption of TiO_2 material. Accordingly, this absorption feature suggested that the photocatalyst can possibly be activated by visible light.

Photocatalytic degradation of phenol at boron-doped TiO_2 mesoporous materials

Figure 5 compared the photocatalytic degradation of phenol at TiO_2 mesoporous materials doped with 0, 1, 2, 3, 5, 7, 10, 15% atom ratio of boron. It can be seen that the boron-doped TiO_2 exhibited much higher photocatalytic activity than pure TiO_2. The 5% B-doped TiO_2 photodegraded about 97% phenol after 240-min irradiation. While at the same condition, pure TiO_2 degraded only about 74% phenol. The photocatalytic activity of the boron-doped TiO_2 mesoporous material increased with the boron doping until boron doping approached to 5% atom ratio. Further increase in boron doping decreased its photocatalytic activity.

The incorporation of boron atoms into TiO_2 extended the spectral response to the visible region. More lights (UV light in addition to some visible light) can be absorbed to produce more photogenerated electrons and more photogenerated holes, and thus increased the photocatalytic activity of boron-doped TiO_2. However, as the boron doping level further increased, more borons doped in the TiO_2 lattice can be functioned as recombination centers of photogenerated electrons and photogenerated holes, which facilitating their recombination. Therefore, the photocatalytic activity of boron-doped TiO_2 was decreased when the doping level is higher than 5%.

Mechanisms of the photocatalytic degradation of phenol at TiO_2 and $TiO_{2-x}B_x$

The UV–vis absorption spectra of phenol degradation by-products at TiO_2 and $TiO_{2-x}B_x$ were compared in Fig. 6. At TiO_2, besides the undegraded phenol peak at 270 nm, a new peak at 289 nm appeared, which was attributed to the ring-retaining compounds such as catechol and hydroquinone (Hosseini et al. 2007; Liu et al. 2008; Emilio et al. 2006; Tryba et al. 2006). However, at $TiO_{2-x}B_x$, besides the phenol peak at 270 nm and the ring-retaining compounds peak at 289, there were two new peaks at 247 and 256 nm, which are attributed to ring-opened products (Tryba et al. 2006; Wang et al. 2008). So, it can be concluded that the mechanism of the photocatalytic degradation of phenol at $TiO_{2-x}B_x$ is different from that of TiO_2. Then, what is the mechanism of phenol degradation at $TiO_{2-x}B_x$?

Phenol decomposition could follow different pathways, giving different by-products. Ilisz et al. investigated the mechanism of phenol decomposition in a TiO_2 aqueous suspension under UV irradiation in the presence of

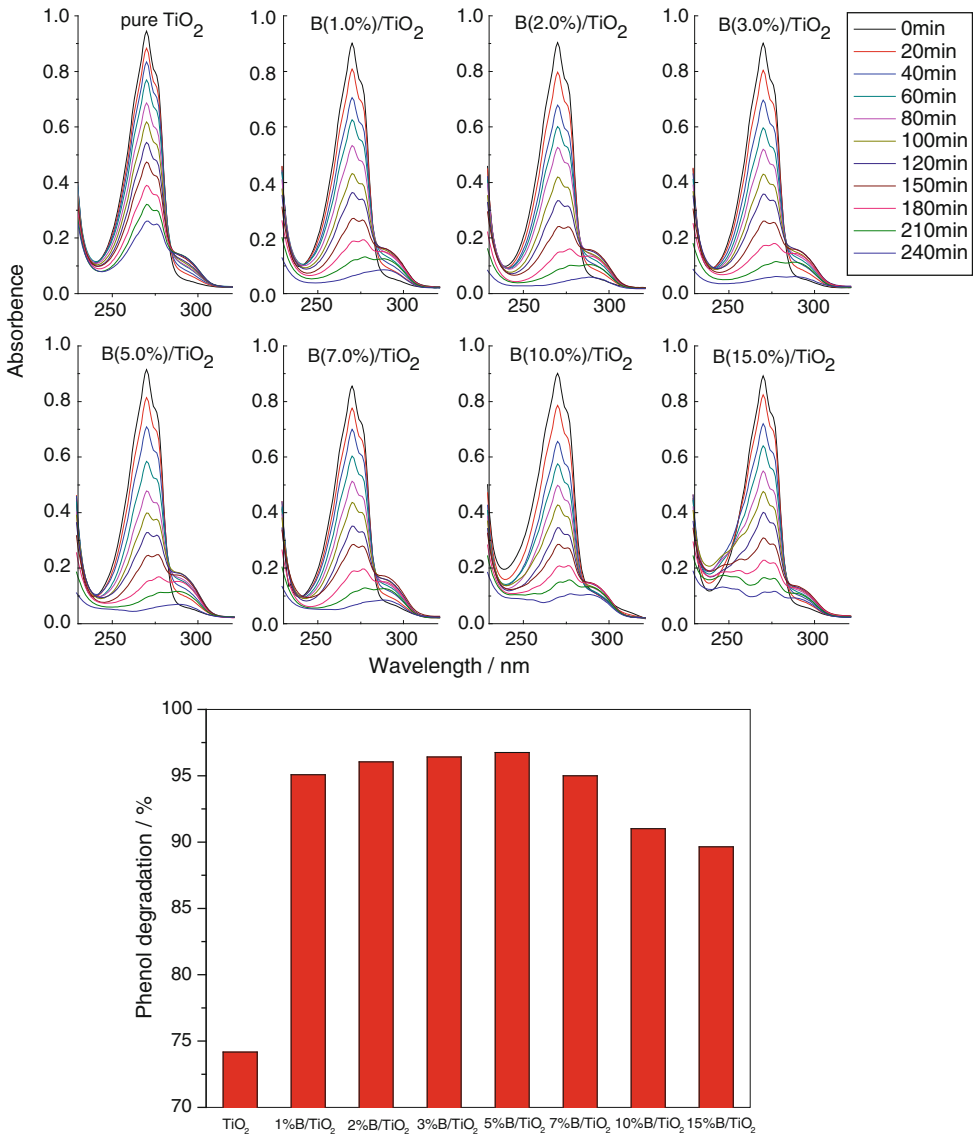

Fig. 5 *Upper*: UV–vis absorption curves of phenol degradation catalyzed by TiO_2 mesoporous materials doped with boron (0, 1.0, 2.0, 3.0, 5.0, 7.0, 10.0, 15.0 atomic %). *Below*: Comparison of phenol degradation rate after 240-min irradiation in the TiO_2 mesoporous materials

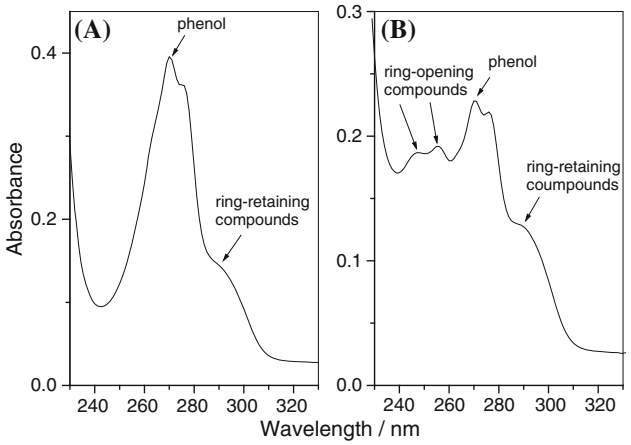

Fig. 6 Characteristic UV–vis absorption spectra of phenol degradation products after 180-min irradiation at TiO_2 (**a**) and 5.0% boron-doped TiO_2 (**b**)

different electron scavengers (Ilisz and Dombi 1999). They found that, in the presence of dissolved oxygen, phenol was decomposed by radical oxidation of •OH, where by-products such as hydroquinone and catechol were detected. In the presence of Ag, phenol was decomposed by direct oxidation with holes. In the presence of H_2O_2, phenol was decomposed by both radical oxidation with •OH and direct oxidation with holes, which proceeded parallel.

In Fig. 7, we proposed two mechanisms of phenol degradation. The first one is radical reaction: photogenerated holes h^+_{vb} first reacted with OH^- groups or adsorbed H_2O at the surface of TiO_2 to produce surface-bound hydroxyl radicals (•OH) through an electron transfer pathway. The hydroxyl radicals then reacted with phenol to produce catechol and hydroquinone, and catechol and hydroquinone were further degraded to carbon dioxide and water. The second one is hole reaction: photogenerated

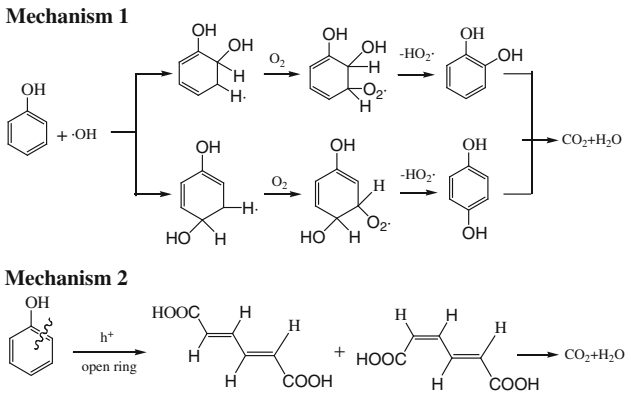

Fig. 7 Two proposed mechanisms on photocatalytic degradation of phenol

holes first reacted directly with phenol adsorbed at the surface of TiO_2. Then, phenol was opened ring to produce 2,4-hexadiendioic acid by the strong oxidant h^+_{vb}, and 2,4-hexadiendioic acid was further degraded to carbon dioxide and water. According to the results in Fig. 6, we believe that phenol degradation at TiO_2 follows radical reaction mechanism. The phenol degradation at $TiO_{2-x}B_x$ follows both radical reaction mechanism and hole reaction mechanism, which proceed parallel. And hole reaction mechanism is favored when increasing the amount of doped boron.

The kinetic study on the photocatalytic degradation of phenol

The dependence of $\ln(C_0/C)$ on the irradiation time t in TiO_2 doped with different ratio of boron was shown in Fig. 8. It was indicated that the initial degradation of phenol followed the quasi-first-order-type kinetics, as evidenced by the linear relationship between $\ln(C_0/C)$ and irradiation time t. Here, C_0 is the initial concentration of phenol, and C is the concentration of phenol after irradiation for t. The initial rate constant (k) for phenol degradation in pure anatase TiO_2 was calculated 0.0044 min^{-1}. While the initial rate constant (k) for phenol degradation in $TiO_{2-x}B_x$ doped with 5% boron was 0.0084 min^{-1}, which was about twice of that in pure anatase TiO_2. The enhancement of catalytic activity on the $TiO_{2-x}B_x$ mesoporous material can be attributed to the shift of optical response to visible region and the high surface area of mesoporous structure. Further increase in boron doping decreased its photocatalytic activity, which indicated that the optimal doping level of boron is 5%.

Boron doped in TiO_2 (atom ratio)	0	1.0%	2.0%	3.0%	5.0%	7.0%	10.0%	15.0%
k / min^{-1}	0.0044	0.0075	0.0076	0.0080	0.0084	0.0068	0.0064	0.0063

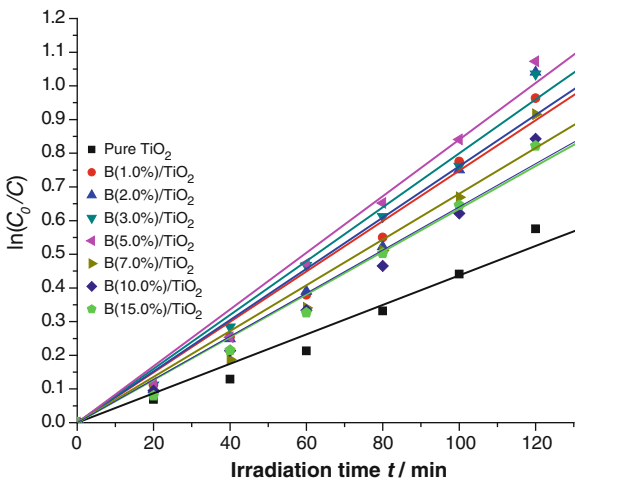

Fig. 8 The dependence of $\ln(C_0/C)$ on the irradiation time t in TiO_2 doped with different ratio of boron. *Inset*: The corresponding initial rate constant (k) of phenol degradation

Conclusions

In summary, we developed a facile approach for preparing $TiO_{2-x}B_x$ mesoporous materials. The porous carbon with high surface area, which was formed by the dehydration of glucose by concentrated sulfuric acid, was used as hard template. The as-synthesized $TiO_{2-x}B_x$ mesoporous materials were well characterized by XRD, BET, TEM, EDX, XPS, and UV–vis spectroscopy. The boron-doped TiO_2 was in pure anatase crystallite phase with high surface area. The absorption spectra of $TiO_{2-x}B_x$ extended into the visible region, which is due to that boron atom was incorporated into the anatase TiO_2 lattice. $TiO_{2-x}B_x$ exhibited much higher photocatalytic activity on phenol degradation than pure TiO_2 and that the phenol degradation by-products of $TiO_{2-x}B_x$ were different from that of pure TiO_2. The photocatalytic degradation of phenol at $TiO_{2-x}B_x$ may proceed by a parallel mechanism, in which photogenerated holes and hydroxyl radicals react with phenol simultaneously.

Acknowledgments This work was financially supported by the National Natural Science Foundation of China (No. 20965003), the Natural Science Foundation of Jiangxi Province (Grant No. 2009), Jiangxi Jinggang-Star Program for Excellent Talents (Grant No. 2008DQ01000), and the Science and Technology Program from Jiangxi Provincial Department of Education (Grant No. GJJ08246).

References

Asahi R, Morikawa T, Ohwaki T, Aoki K, Taga Y (2001) Visible-light photocatalysis in nitrogen-doped titanium oxides. Science 293(5528):269–271

Batzill M, Morales EH, Diebold U (2006) Influence of nitrogen doping on the defect formation and surface properties of TiO_2 rutile and anatase. Phys Rev Lett 96(2):026103

Bavykin DV, Friedrich JM, Walsh FC (2006) Protonated titanates and TiO_2 nanostructured materials: synthesis, properties, and applications. Adv Mater 18(21):2807–2824

Bettinelli M, Dallacasa V, Falcomer D, Fornasiero P, Gombac V, Montini T, Romano L, Speghini A (2007) Photocatalytic activity of TiO_2 doped with boron and vanadium. J Hazard Mater 146(3):529–534

Boettcher SW, Fan J, Tsung CK, Shi QH, Stucky GD (2007) Harnessing the sol-gel process for the assembly of non-silicate mesostructured oxide materials. Acc Chem Res 40(9):784–792

Carp O, Huisman CL, Reller A (2004) Photoinduced reactivity of titanium dioxide. Prog Solid State Chem 32(1–2):33–177

Chen XB, Burda C (2008) The electronic origin of the visible-light absorption properties of C-, N- and S-doped TiO_2 nanomaterials. J Am Chem Soc 130(15):5018–5019

Chen YS, Crittenden JC, Hackney S, Sutter L, Hand DW (2005) Preparation of a novel TiO_2-based p-n junction nanotube photocatalyst. Environ Sci Technol 39(5):1201–1208

Chenthamarakshan CR, Rajeshwar K (2000) Heterogeneous photocatalytic reduction of Cr(VI) in UV-Irradiated titania suspensions: effect of protons, ammonium ions, and other interfacial aspects. Langmuir 16(6):2715–2721

Di Valentin C, Finazzi E, Pacchioni G, Selloni A, Livraghi S, Paganini MC, Giamello E (2007) N-doped TiO_2: theory and experiment. Chem Phys 339(1–3):44–56

Emilio CA, Litter MI, Kunst M, Bouchard M, Colbeau-Justin C (2006) Phenol photodegradation on platinized-TiO photocatalysts related to charge-carrier dynamics. Langmuir 22(8):3606–3613

Ho W, Yu JC, Lee S (2006) Synthesis of hierarchical nanoporous F-doped TiO_2 spheres with visible light photocatalytic activity. Chem Commun (10): 1115–1117

Hoffmann MR, Martin ST, Choi WY, Bahnemann DW (1995) Environmental applications of semiconductor photocatalysis. Chem Rev 95(1):69–96

Hosseini SN, Borghei SM, Vossoughi M, Taghavinia N (2007) Immobilization of TiO_2 on perlite granules for photocatalytic degradation of phenol. Appl Catal B 74(1–2):53–62

Huang Y, Ho WK, Lee SC, Zhang LZ, Li GS, Yu JC (2008) Effect of carbon doping on the mesoporous structure of nanocrystalline titanium dioxide and its solar-light-driven photocatalytic degradation of NO_x. Langmuir 24(7):3510–3516

Ilisz I, Dombi A (1999) Investigation of the photodecomposition of phenol in near-UV irradiated aqueous TiO2 suspensions II. Effect of charge-trapping species on product distribution. Appl Catal A 180(1–2):35–45

In S, Orlov A, Berg R, Garcia F, Pedrosa-Jimenez S, Tikhov MS, Wright DS, Lambert RM (2007) Effective visible light-activated B-doped and B, N-codoped TiO2 photocatalysts. J Am Chem Soc 129(45):13790–13791

Khan SUM, Al-Shahry M, Ingler WB (2002) Efficient photochemical water splitting by a chemically modified n-TiO_2. Science 297(5590):2243–2245

Li YZ, Hwang DS, Lee NH, Kim SJ (2005) Synthesis and characterization of carbon-doped titania as an artificial solar light sensitive photocatalyst. Chem Phys Lett 404(1–3):25–29

Lin L, Lin W, Zhu YX, Zhao BY, Xie YC (2005) Phosphor-doped titania—a novel photocatalyst active in visible light. Chem Lett 34(3):284–285

Liu SX, Chen XY (2008) A visible response TiO_2 photocatalyst realized by cationic S-doping and its application for phenol degradation. J Hazard Mater 152(1):48–55

Liu L, Liu HJ, Zhao YP, Wang YQ, Duan YQ, Gao GD, Ge M, Chen W (2008) Directed synthesis of hierarchical nanostructured TiO catalysts and their morphology-dependent photocatalysis for phenol degradation. Environ Sci Technol 42(7):2342–2348

Livraghi S, Paganini MC, Giamello E, Selloni A, Di Valentin C, Pacchioni G (2006) Origin of photoactivity of nitrogen-doped titanium dioxide under visible light. J Am Chem Soc 128(49): 15666–15671

Lu N, Quan X, Li JY, Chen S, Yu HT, Chen GH (2007) Fabrication of boron-doped TiO_2 nanotube array electrode and investigation of its photoelectrochemical capability. J Phys Chem C 111(32): 11836–11842

Nakano Y, Morikawa T, Ohwaki T, Taga Y (2005) Electrical characterization of band gap state in C-doped TiO_2 films. Appl Phys Lett 87(5):052111

Nishijima K, Fujisawa Y, Murakami N, Tsubota T, Ohno Y (2008) Development of an S-doped titania nanotube (TNT) site-selectively loaded with iron(III) oxide and its photocatalytic activities. Appl Catal B 84(3–4):584–590

Soler-illia GJD, Sanchez C, Lebeau B, Patarin J (2002) Chemical strategies to design textured materials: from microporous and mesoporous oxides to nanonetworks and hierarchical structures. Chem Rev 102(11):4093–4138

Soni SS, Henderson MJ, Bardeau JF, Gibaud A (2008) Visible-light photocatalysis in titania-based mesoporous thin films. Adv Mater 20(8):1493–1498

Tryba B, Morawski AW, Inagaki M, Toyoda M (2006) The kinetic of phenol decomposition under UV irradiation with and without H_2O_2 on TiO_2, Fe-TiO_2 and Fe-C-TiO_2 photocatalysts. Appl Catal B 63(3–4):215–221

Wang H, Lewis JP (2005) Effects of dopant states on photoactivity in carbon-doped TiO2. J Phys Condens Matter 17(21):L209–L213

Wang JB, Zhu WP, Yang SX, Wang W, Zhou YR (2008) Catalytic wet air oxidation of phenol with pelletized ruthenium catalysts. Appl Catal B 78(1–2):30–37

Wold A (1993) Photocatalytic properties of TiO_2. Chem Mater 5(3):280–283

Wu GS, Wang JP, Thomas DF, Chen AC (2008) Synthesis of F-doped flower-like TiO_2 nanostructures with high photoelectrochemical activity. Langmuir 24(7):3503–3509

Xu CK, Khan SUM (2007) Photoresponse of visible light active carbon-modified-n-TiO_2 thin films. Electrochem Solid State Lett 10(3):B56–B59

Xu JJ, Ao YH, Fu DG, Yuan CW (2008) Low-temperature preparation of F-doped TiO_2 film and its photocatalytic activity under solar light. Appl Surf Sci 254(10):3033–3038

Yang K, Dai Y, Huang BB (2007) Origin of the photoactivity in boron-doped anatase and rutile TiO_2 calculated from first principles. Phys Rev B 76(19):195201

Yu JC, Ho WK, Yu JG, Yip H, Wong PK, Zhao JC (2005) Efficient visible-light-induced photocatalytic disinfection on sulfur-doped nanocrystalline titania. Environ Sci Technol 39(4):1175–1179

Zaleska A, Sobczak JW, Grabowska E, Hupka J (2008) Preparation and photocatalytic activity of boron-modified TiO_2 under UV and visible light. Appl Catal B 78(1–2):92–100

Zhao W, Ma WH, Chen CC, Zhao JC, Shuai ZG (2004) Efficient degradation of toxic organic pollutants with $Ni_2O_3/TiO_{2-x}B_x$ under visible irradiation. J Am Chem Soc 126(15):4782–4783

Zheng RY, Lin L, Xie JL, Zhu YX, Me YC (2008) State of doped phosphorus and its influence on the physicochemical and photocatalytic properties of P-doped titania. J Phys Chem C 112(39):15502–15509

Zhou JK, Lv L, Yu JQ, Li HL, Guo PZ, Sun H, Zhao XS (2008) Synthesis of self-organized polycrystalline F-doped TiO_2 hollow microspheres and their photocatalytic activity under visible light. J Phys Chem C 112(14):5316–5321